Liquefaction-Induced Lateral Spreading

Earthquake-induced ground deformations within the depth of engineering significance are related to either fault surface rupture or ground motion. In geotechnical engineering applications, ground deformations are usually reported in terms of vertical and horizontal components, which are commonly referred to as *settlements* and *lateral deformations,* respectively. The terms *lateral deformation, lateral displacement* and *lateral movement* are often used interchangeably without any distinction. Earthquake-induced ground deformations can occur in both liquefied and non-liquefied soils. However, relatively large seismic lateral ground movements that can cause collapse or failure of highway facilities, including bridges, slopes and earth retaining structures (ERS) are most often associated with soil liquefaction. The scope of this module is limited to this type of relatively large seismic lateral ground deformation, a phenomenon commonly referred to as "*liquefaction-induced lateral spreading.*"

Unless specified otherwise in a Project-Specific Seismic Design Criteria (PSDC), this module is applicable to bridges designed or required to be retrofitted in accordance with the Caltrans Seismic Design Criteria (SDC), and other appurtenant highway facilities including ERS, slopes and embankments.

Background

The phenomenon of "*liquefaction-induced lateral spreading"* during earthquakes has been defined and interpreted variably in the research literature as well as in practice.

Liquefaction-induced lateral spreading was identified and documented as one of the main causes of damage to highway facilities during strong earthquakes in the late 19th century but did not receive much attention until the late 20th century. However, significant progress has since been made on the subject of predicting the occurrence of soil liquefaction at project sites during future earthquakes. The fundamental soil mechanics principles and other important factors associated with soil liquefaction during earthquakes has since been identified and extensively studied, and prediction methods developed that are now widely used in practice.

Liquefied soils can experience a significant reduction in shear strength, which in turn can cause a drastic reduction in the static soil lateral resistances available to support a sloped or mechanically restrained soil masses (e.g., bridge abutment, retaining wall etc.) that are subjected to sustained destabilizing static shear stresses. As a result, such soil masses often experience large permanent lateral movements (or spreading) during or immediately after earthquake-induced ground shaking. California is one of the highly active seismic regions of the world, and liquefaction-induced lateral spreading of grounds poses a serious threat to bridges and other transportation facilities.

Lateral spreading hazards, particularly at bridge support locations, have been intensely researched during recent decades. The subject, however, has proven to be difficult,

specifically for sites with mechanically restrained ground due to the complex seismic soil-foundation-structure interaction mechanisms involved.

Caltrans has been considering lateral spreading hazards at project sites based on the rapidly evolving state of the art knowledge. Recently, the Department published MTD 20-15 documenting a recommended lateral spreading hazard analysis procedure for deep-foundation supported new and existing bridges. The recommended procedure involves both geotechnical and structure analyses in an iterative manner and requires common understanding and timely communications between the project Geotechnical Designer (GD) and the Structure Designer (SD).

This module presents the underlying basic geotechnical concepts to facilitate a thorough and uniform understanding among the geo-professionals of the fundamental mechanisms involved with liquefaction-induced lateral spreading, and of related Caltrans' current analysis and design practices. The state-of-knowledge as well as the state-of-practice regarding lateral spreading is rapidly evolving. As such, this module will be updated periodically as new information becomes available.

The geotechnical scope of work associated with a liquefaction-induced lateral spreading hazard analysis for a project involves the evaluation of site-specific soil liquefaction hazards, residual shear strength of liquefied soils, ground lateral or slope stability and permanent lateral ground displacements. Several analysis procedures are available for the evaluation of earthquake-induced soil liquefaction hazards at a project site. For Caltrans projects, soil liquefaction is evaluated in accordance with the procedure in the "*Soil Liquefaction Evaluation"* module of the Geotechnical Manual (GM).

At this time, the relevant ground motion parameters for both liquefaction evaluation and lateral spreading analysis, include the Horizontal Peak Ground Accelerations (PGA) and the moment magnitude (M) of the associated earthquake event. For Safety Evaluation Earthquake (SEE), as defined in SDC, the design horizontal PGA corresponds to a return period of 975-years. For clarity, the design Horizontal PGA (in g) is referred to herein as the design HPGA (in g), where g is the acceleration of gravity. The design earthquake magnitude (M) is taken as equal to the moment magnitude of the deaggregated mean earthquake for the design HPGA. Other aspects of a liquefaction-induced lateral spreading analysis are discussed in the following sections.

Liquefaction-Induced Lateral Spreading

In general, soil masses under the influence of static driving shear stresses, such as sloping grounds, ERS and bridge abutments, are susceptible to liquefaction-induced lateral spreading during earthquakes.

The seismic phenomenon of small (1.0 inch) to very large (>30 ft) permanent lateral ground deformation involving liquefied soils, termed as the *liquefaction-induced lateral spreading,* can be divided into three broad categories:

- Moderate to steeply sloping or mechanically retained soil masses, including embankment slopes, ERS and bridge abutments, are susceptible to flow type landslides when the available reduced lateral sliding resisting capacities (or lateral nominal sliding resistances) due to soil liquefaction falls below the destabilizing total lateral static driving forces. In such cases, the soil mass experiences a large lateral displacement or movement. The magnitude of such large lateral movement is unpredictable. For all practical purposes, such soil mass can be considered to have experienced unlimited lateral movement, and thus have failed or collapsed. This type of ground failure is termed as a *flow failure*, which usually occurs after the cessation of the ground shaking. Once initiated, the magnitude of the lateral movement that such a soil mass may experience is independent of the ground motion parameters.

- In the case where the reduced residual lateral resisting capacity remains greater than the total destabilizing static lateral forces, the soil mass experiences, if any, limited lateral ground deformations or movements during ground shaking. Such lateral movement occurs in an incremental manner during only those seismic inertial loading cycles when the total (static +seismic) destabilizing lateral load exceeds momentarily the available reduced total lateral resistance. The soil mass stop moving as soon as the total lateral load falls below the available total resistance due to reduction in the inertial lateral load. The soil mass may experience large but limited lateral displacement before coming to a full stop at or before the cessation of the ground shaking. In liquefied soils, this type of lateral ground displacement or lateral spreading occurs during ground shaking under the combined effects of the reduced shear strength and the lateral inertial forces.

- During past major earthquakes, relatively thin surficial blocks of mildly sloping ground and flat ground with free boundary surface, mostly near water bodies with shallow groundwater, have experienced liquefaction-induced small to very large downslope ground movements. Little or no static driving shear stresses exist in these type of soil masses. Lateral ground deformations occurred mainly due to the accumulation of ground motion-induced cyclic shear strains within a shallow or surficial liquefied soil layer.

  Non-liquefied soil crust layers overlying the liquefied layer, where present, may experience additional compressional deformation in the downslope direction due to self-weight and inertial forces. The overlying soil crust may simply ride downslope on its contact with the underlying liquefied soil layer. In this case, the underlying liquefied soil layer acts essentially as a base isolation. This type of permanent lateral ground displacement or lateral spreading can occur both during and immediately after the cessation of the ground motion.

Shear Strength of Liquefied Soils

Stress-Strain Behavior During Undrained Monotonic Loading

Saturated, loose to medium dense cohesionless soils with little or no plastic fines develop positive excess pore water pressure (Δu) due to the cyclic shear stresses induced by earthquake shaking. These soils tend to contract when sheared but are unable to do so during seismically induced shear loading. This is because the permeability of these soils, compared with the very fast rate of loading, is inadequate to allow drainage to occur during the load application. This in turn results in the development of positive excess pore pressure within these soils during ground shaking. That is, such cohesionless soils may be free draining under normal conditions but behave as undrained (similar to cohesive soil) soils during earthquakes.

The positive excess pore pressure reduces the effective confining stresses in the soils causing significant reductions in the soil shear strengths and stiffnesses during ground shaking. In some cases, fully reduced shear strength and stiffness conditions continue to prevail until sometime well after the cessation of the seismically-induced ground shaking when the generated excess pore pressure starts to dissipate.

Figure 1 depicts schematically, based on original research work performed by Castro (1969), the undrained response of saturated cohesionless soils when sheared monotonically. In these cases, the rate of loading is significantly slow compared to earthquake-induced loading. However, soil contraction or drainage of the porewater from these soils is artificially prevented so that shearing occurs under undrained conditions. The effects of the shear loading, despite slower rate but being undrained, would be expected to be like those during fast seismically-induced shear loading. Understanding these fundamental aspects of the undrained shear behavior of saturated cohesionless soils is a basic prerequisite for understanding soil liquefaction during earthquakes and its potential impacts on the deformation and stability of grounds as well as the facilities constructed of, within or on these types of soils.

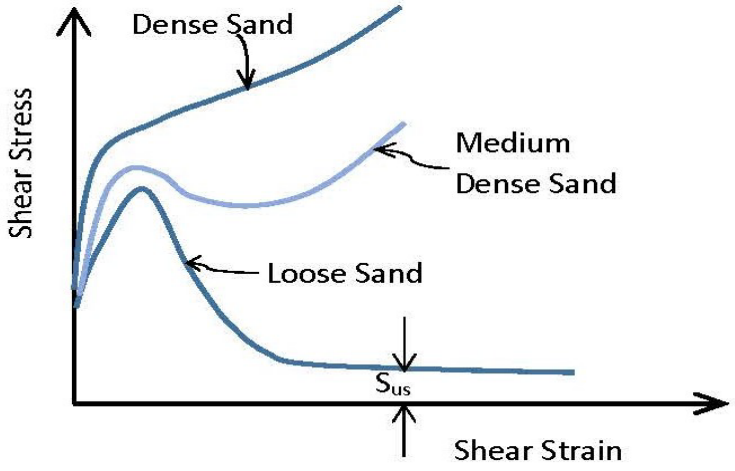

Figure 1: Undrained Shear Stress-Strain Behavior of Saturated Cohesionless Soils Under Monotonic Loading (Schematic)

Point A in Figure 1 represents the *initial states* of the three (3) saturated sand soil samples sheared monotonically under undrained conditions. For the loose sand sample, as the applied shear stress, over the sustained static shear stress (τ_s), increases, the excess pore pressure also increases. The shear stress-strain curve quickly reaches a peak, which is equal to the *peak undrained shear strength* $(S_u)_{peak}$ of the soil. After this point the applied shear stress that the soil can sustain starts to decrease rapidly until it drops to a minimum value (S_{us}) at some large strain. At this point, the loose sand continues to experience shear deformation at a constant rate without any increase or decreases in the applied shear stresses. This state of soil, defined in term of the soil density (which is the same as the initial density) and the operating effective confining stress, is termed as the steady state (Poulos and Castro, 1974).

When the undrained shear strength, after attaining the peak value, drops to the minimum value, the loose soil is said to have completely liquefied since beyond this point the undrained soil shears like a liquid. The available minimum undrained unit shear resistance for a completely liquefied soil is termed as the *steady state shear strength* (S_{us}) of the soil (Poulos and Castro, 1974) (Figure 1).

At the instant the peak undrained shear strength is exceeded, the loose sand is said to have experienced initial liquefaction or liquefaction triggering. In completely liquefied soils, the excess pore water pressure continues to rise during further shearing until the undrained shear strength drops to the steady state shear strength, which remains the same during further undrained shearing.

The saturated, medium dense sand, (Figure 1) initially behaves in a manner very similar to the loose sand. The medium dense sand experiences initial liquefaction and then shear resistance drops to a minimum value. However, the medium dense sand experiences less reduction in the available undrained shear strength after reaching the initial peak strength (i.e., initial liquefaction). Furthermore, the minimum undrained shear strength for the medium dense sand is reached at a lower shear strain than the loose sand.

Most significantly, soon after reaching the minimum shear strength condition, the undrained shear resistance of the medium dense sand starts to increase again. This occurs because after experiencing the minimum shear strength condition, the state (the combination of density and stresses or strains) of this medium dense sand has transitioned from a tendency to contract to a tendency to dilate, which in turn results in the reduction of the pores water pressure. From this point on, due to continued tendency of the soil to dilate as the sample is further sheared, the pore water pressure continues to decrease, which in turn results in a continued increase in the undrained shear resistance of the soil.

In Figure 1, both the loose and the medium sand have experienced initial liquefaction. However, the medium dense sand regained its pre-initial liquefaction peak shear strength after a small amount of post-initial liquefaction shear deformation. Upon further shearing, the undrained shear strength of the medium dense continues to increase above the initial peak undrained shear strength. Whereas the undrained shear strength of the loose sand not only drops to a much lower minimum undrained shear strength and at a much larger

shear deformation, further shearing does not result in an increase in the undrained shear strength. The loose sand sample continues to shear at constant effective confining stress, that is, the undrained shear strength remains the same.

As soon as the available undrained shear strength, after reaching the peak, dropped below the sustained static shear stress (τ_c), the loose sand essentially collapsed, and experienced uncontrolled viscous fluid flow causing large shear deformation. This type of undrained shear behavior experienced by saturated loose sand is termed as "*Flow Liquefaction."* The undrained shear behavior exhibited by the medium dense sand is termed as "*Limited Liquefaction.*"

On the other hand, as shown in Figure 1, the undrained stress-strain response of the saturated dense cohesionless soil sample is characterized by a stiff curve with no reduction in the available undrained shear resistance during shearing. Such soils are thus considered not susceptible to liquefaction or significant lateral deformations during earthquakes.

Note that the undrained shear stress-strain response of a given saturated cohesionless soil depends on its initial state defined in terms of the initial density and initial effective confining stress. Depending on the combination of these two major controlling parameters or the initial state, the undrained stress-strain responses will transition gradually from one type of behavior to the others (Figure 1). No simple criteria exist that can be used to distinctly delineate the boundaries between the three typical types of undrained behavior of saturated cohesionless soils depicted in Figure 1.

It can be seen from the above that the initial density (or the initial relative) alone can not be used to predict the undrained stress-strain behavior or liquefaction susceptibility of a cohesionless soil. It the initial state, i.e., the combination of the initial density (or initial relative density) and the initial effective confining stress, of a given saturated cohesionless (or sand-like) soil that controls its undrained shear behavior or liquefaction susceptibility during earthquakes. The amount of lateral deformations that a liquefied soils may experience also depends on additional factors, including the destabilizing sustained or initial static shear stress or topography, drainage and boundary conditions (e.g., free face versus laterally supported earth mass) as well as the magnitude, frequency content, duration and other characteristics of the earthquake induced base ground motion as well as the ground motion experienced by the laterally spreading soil mass.

Case History of Excess Pore Pressure Generation in Liquefied Soil

Figure 2 shows two acceleration-time histories recorded in the field during an actual earthquake event (1987 Superstition Hills Earthquake of M_w=6.6). The recording station was located on a relatively flat soil site. The soil profile at the recording station (known as the Wildlife Site) consists of about a 2.5 m (8.0 feet) thick upper layer of silt to clayey silt soils underlain by a 4.3 m (≅ 14 feet) thick silty sand to sandy silt layer, which in turn is underlain by a 4.7 m (15.5 feet) thick clay layer. The groundwater table at the time of the earthquake was 1.5 m below the ground surface.

The 4.3 m thick silty sand to sandy silt layer (between 2.5 to 6.8 m below the ground surface) liquefied during the recorded seismic event.

Of the two acceleration-time histories recorded at the site (Figure 2a), one was at the surface (depth =0) and the second was at 7.5 m below the ground surface. The excess porewater pressures (Figure 12b) in terms of the ratio r_u, were recorded at four different depths within the 4.0 m thick liquefied soil layer. The symbols P5, P2, P1 and P3 represent the piezometers located at depths of 2.9, 3.0, 5.0 and 6.6 m, respectively.

Zeghal and Elgamal (1994) divided the acceleration-time and the excess porewater pressure ratio-time histories (Figure 2) into four stages in term of time starting from the onset of ground shaking.

During Stage 1 (0.0 to 13.7 sec), ground acceleration amplitude was low and the excess porewater pressures at all depths within the liquefied soil layer increased slowly a small amount.

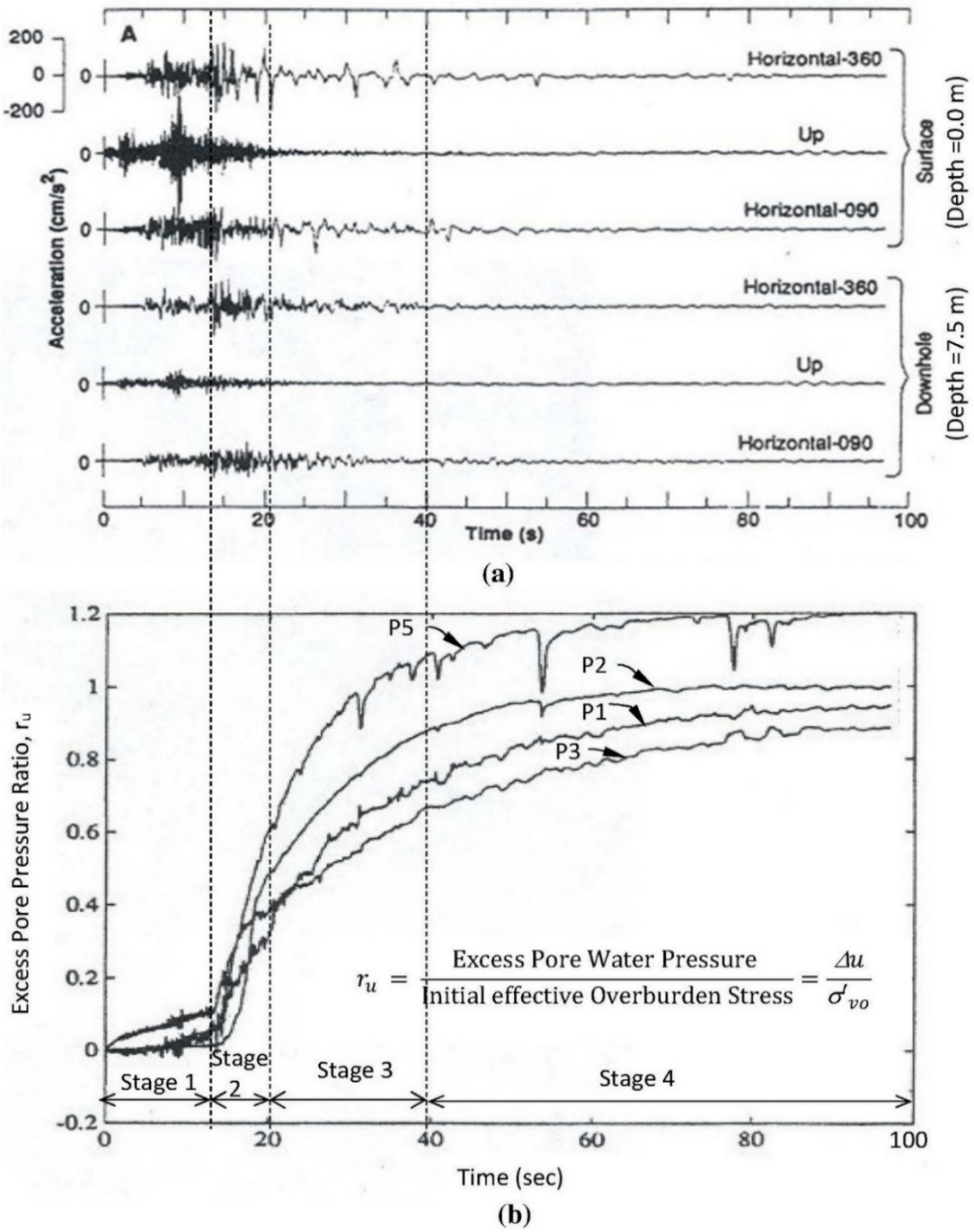

Figure 2: Results of Field Monitoring of the Wildlife Array Instruments During the 1987 Superstition Hills Earthquake: (a) Recorded Traces of Accelerations and Pores Pressures; (b) Recorded Pore Pressure as a Ratio of the Estimated Initial Effective Overburden Stress Versus Time (Modified after Holzer et al., 1989, Dobry et al., 1989 and Youd and Carter, 2005)

During Stage 2 (13.7 to 20.6 sec) the ground motion was intense during which time the PGA values of 0.17g and 0.21 g, occurred at 7.5 m and 0.0 m depths, respectively. During this shaking period, excess pore pressure increased rapidly.

During Stage 3 (20.6 to 40.0 sec), ground motion intensity was lower with the maximum acceleration of about 0.06g. The excess pore-pressure, however, continued to increase rapidly. At the end of the 3rd Stage, the excess pore pressures reached relatively high magnitudes.

During Stage 4 (40.0 to 96 sec) the ground motion intensity was low. The excess pore pressure continues to rise, albeit at a much slower rate, until the end of shaking.

The ground motion records in Figure 2(a) show that for all practical purposes the earthquake-induced input ground motion at the base of the liquefied soil layer (at depth 7.5 m) ended about 40 to 50 seconds after the onset of the ground motion. Note, however, that the excess pore pressure (Figure 2b) continues to increase (or at least did not start to drop or dissipate) for sometimes well after 40 to 50 seconds or the cessation of ground motion at the non-liquefiable base layer (at 7.5 m depth).

The characteristics of ground motion records at the surface (Figure 2a) and the excess pore pressure records (Figure 2b) indicate that the 4.3 m thick silty sand and sand silty layer, sandwiched between two non-liquefiable soil layers, experienced initial liquefaction (or triggering) at about the time the average excess pore pressure ratio of about 0.45 to 0.5 for the entire layer.

Residual Shear Strength of Liquefied Soils

The analysis procedure in the “Liquefaction Evaluation” module of the Geotechnical Manual predicts whether potentially liquefiable soils at a project site will experience initial liquefaction due to the specified design HPGA (and the design M) at the ground surface obtained by assuming no liquefaction.

In liquefied soils that are susceptible to lateral spreading displacements of magnitudes significant for the SEE seismic design, i.e., to cause seismic failure or collapse of ground or structures, the excess pore pressure during the seismic event is likely to continue to increase (positive) past initial liquefaction until the excess pore pressure ratio (r_u) reaches a high value close or equal to 1.0. The excess pore pressure ratio, r_u, at any soil depth is defined as the ratio of the excess pore pressure (Δu) to the initial effective overburden stress (σ'_{vo}) (Figure 2). These types of soils are highly susceptible to liquefaction, as would generally be predicted as such by the relatively low value of the corrected and normalized clean-sand equivalent SPT blow count $(N_1)_{60\text{-}cs}$ as defined in Youd et al (2001) or the normalized clean-sand equivalent CPT cone tip resistance, ($Q_{tn,\,cs}$) as defined in Robertson (2009). Note that Q_{tn} = Q as defined in Youd et al (2001), and $Q_{tn.cs} = K_c\, Q_{tn}$. Here K_c, the correction factor for grain characteristics (combined influence of fines content, mineralogy, and plasticity) and $(N_1)_{60\text{-}cs}$ are as defined in Youd et al (2001).

Studies of a large numbers of case-histories (Bartlett et al, 1995, Kramer and Wang, 2015, Robertson, 2009) also indicated that almost all cases of liquefaction-induced lateral spreading involving significant lateral ground displacements, including flow failures, have been limited to liquefied soils with $(N_1)_{60\text{-}cs} \leq 15$ or $Q_{tn,cs} \leq 70$.

Therefore, it can be assumed that in liquefied soils that are likely to experience significant liquefaction-induced lateral spreading displacements, the excess pore water pressure either continues to rise slowly or remains at about the same, after reaching a peak r_u value equal or close to 1.0 during ground shaking, until the cessation of ground shaking.

The contractiveness of a cohesionless soil deceases with increase in $(N_1)_{60\text{-}cs}$, which represent the equivalent *initial state* of a clean sand. As $(N_1)_{60\text{-}cs}$, increases, for example to slightly above 15, the liquefaction behavior of a clean sand transitions from complete or flow type to near-complete or somewhat limited liquefaction. The excess pore pressure in such soil drops, if any, only slightly due to dilation after reaching a significantly high peak r_u value (i.e., close to 1.0) during the ground shaking period. These types of liquefied soils may experience relatively large but limited lateral spreading.

As $(N_1)_{60\text{-}cs}$ further increases, the contractiveness and the peak r_u value of a granular soil continue to decrease. A clean sand that is only somewhat to slightly contractive, for example when $(N_1)_{60\text{-}cs}$ is in the range of 20-25 may experience even smaller peak R_u value but sufficiently high for the initial liquefaction to occur during ground shaking. However, the initial liquefaction of such soils will be immediately followed by a significant drop in the excess pore pressure due to its transition from the contractive to dilative state. These types of soils even when identified as liquefiable based on the prediction of initial liquefaction (or liquefaction triggering) are not susceptible to significant lateral spreading displacements.

In general, any reduction in the excess pore pressure either due to dilation or drainage after reaching the peak during shaking will result in less deformation than if there were no such reduction during shaking. Thus, for lateral spreading analysis it is conservative to assume that liquefied soils experience no pore pressure reduction after reaching the peak and until after the cessation of ground shaking or inertial loading.

In summary, it can be assumed that fully liquefied soils are susceptible to significant lateral spreading displacements, including flow failures.

Like the loose sand sample (Figure 1), field soils that experience full or complete liquefaction during earthquake shaking retain a certain minimum amount of undrained shear resistance even after experiencing very large shear displacements. For the ideal field case, this minimum shear strength should be the same as the steady state shear strength (S_{us}) for the same soil. In practice, the ideal laboratory testing conditions may not occur, and it is very difficult to evaluate the steady state shear strengths in both the laboratory and the field. As a result, significant research has been conducted to estimate the average minimum shear strengths that were operating in the field when lateral spreading occurred during past earthquakes. The minimum shear strength thus evaluated is termed as the undrained residual shear strength (S_r) of the liquefied soils.

Based on these efforts, several correlations have been proposed between S_r and the corrected and normalized field measured SPT blow count $N1_{60}$ (and CPT tip resistance) with or without fines-corrections.

For a given soil the magnitude of S_r, like S_{us}, depends only on the "initial state", defined in terms of the initial density and initial effective overburden stress. For projects, the empirical correlation proposed by Kramer and Wang (2015), is recommended in MTD 20-15 to evaluate S_r of the soils that are predicted to liquefy and are susceptible to liquefaction-induced lateral spread hazards when subjected to the design ground motions:

$$S_r(\text{psf}) = 2116 \exp\left\{-8.444 + 0.109N_{1_{60}} + 5.379\left(\frac{\sigma'_{vo}}{2116}\right)^{0.1}\right\} \quad (1)$$

Where,

$N1_{60}$ = Energy corrected and overburden pressure normalized SPT blow count at the depth under consideration. The field measured SPT blow count (N_m) at any depth is corrected to standard 60% hammer engery and normalized to an initial effective overburden stress equal to one (1.0) atmospheric pressure (≅ 2116 psf). See "Liquefaction Module" of the Geotechncial Manual for a detailed calculation procedure for $N1_{60}$.

σ'_{vo} = Initial in-situ effective overburden stress at the depth under consideration evaluated based on the ground surface and groundwater elevations applicable to seismic design (Extreme Event Limit State I).

In the above correlation the normalized SPT blow count $N1_{60}$, represents a measure of the in-situ initial state of the soil. Note that, unlike for the liquefaction hazard evaluation, $N1_{60}$ in the above correlation is ***not*** corrected for fines content.

Design Ground Motion Parameters

Unless specified or required to be specified in a Project-Specific Seismic Design Criteria (PSDC), current seismic design procedure for bridges consists of a Safety Evaluation Earthquake (SEE), as defined in the Seismic Design Criteria (SDC).

Unless a site-specific time-history type analysis is performed, the SEE design ground motions evaluated as per SDC is in the form of a single uniform "Design Spectrum" representing the design horizontal ground motions at the surface of the site corresponding to a return period of 975-years (or 5 percent probability of exceedance in 50 years). MTD 20-1 specifies the acceptable minimum performance criteria for SEE seismic design as "significant damage" and "no collapse" due to the "Design Earthquake".

Currently, for SEE seismic design, the following design ground motion parameters are generally necessary for the analysis and evaluation of liquefaction-induced lateral spreading. As stated earlier, these parameters are determined in accordance with the procedure specified in Appendix B of the SDC.

1) Design HPGA corresponding to a return period of 975-years, and
2) Design earthquake magnitude (M) which is taken as equal to moment magnitude of the deaggregated mean earthquake for the design HPGA, and
3) The deaggregated mean site-to to source distance (R_{rup}) for design HPGA

Hereafter, in this document the moment magnitude of the design earthquake (M) will be referred to as the "Design M". Note that at this time, the design HPGA for lateral spreading analysis is taken as equal to the design spectral acceleration (S_a) at structure period, T=0.0 sec.

Seismic Lateral Stability and Deformation Analysis

For SEE design, steep slopes and earth-retaining system (ERS) with or without mechanical restraining elements (e.g., piles, ground anchors etc.) are usually analysed for seismic lateral instability, including lateral defomations or displacements. Soil liquefaction-induced lateral spreading and other ground distress mechanisms of ground, particularly those involving mechanical lateral resisting elements where soil-foundation-structure interactions play a signficant role, are complex phenomena and the subjects of intense on-going research.

To date, the most pertinent and reliable analysis methodology that can be easily used in the design of common projects has been developed based on work involving unrestained sloping ground that is not affected by soil liquefaction. This methodology involves: (1) A seismic Lateral Stability Analysis. A pseudo-static slope stablity analysis is usually performed to evaluate lateral stability during an earthquake, and when necessary, (2) A lateral displacement analysis as per Newmark Displacement Analysis Method (NDAM). NDSAM provides an estimate of the lateral displacement that occurs during ground shaking.

A brief description of the basic elements of this analysis methodology is presented first in the following section since it provides the necessary background for the methodology included in the MTD 20-15 (2017) for the analysis of liquefaction-induced lateral spreading hazards for new and existing bridges. With regard to the restrained ground or ERS, it should be noted that seismic lateral stability and lateral movements discussed in this module pertain only to the global or overall slope stablity type lateral sliding mechanisms. Lateral sliding hazards along the base of the shallow foundations, where involved, are not covered in this module. However, many of the concepts discussed herein are equally applicable to such cases.

Seismic Lateral Stability Analysis

Seismic Coefficient

Seismic lateral sliding stablity of non-liquefied, moderately to steeply sloping ground and the overall (or global) stability of ERS, including those mechnically restrained by structural elements (e.g., piles, ground anchors, etc.), during earthquake-induced ground shaking events are usually evaluated using a limit-equlibrium based pseudo-static slope stability analysis. Figure 3 presents a typical schematic model to illustrate the basic concepts involved with the limit-equlibrium based pseudo-static slope stability analysis of a slope.

Despite significant limitations, the most commonly practiced analysis procedures to evaluate the first two categories of lateral spreading hazards discussed in the *Liquefaction-Induced Lateral Spreading* section, including the Newmark' rigid body displacement analysis in MTD 20-15, make use of the limit-equlibrium based pseudo-static slope stability analysis.

A pseudo-static slope stablity analysis is a force-based seismic lateral sliding stability analysis utilizing the same limit-equlibirum concept as the one used in static slope stablity analyses.

In a pseudo-static lateral sliding stability analysis, in addition to the applicable sustained or static forces, an additional destablizing dynamic lateral force is applied at the centroid of the mass being analysed for stablity. This additional dynamic force, $F_h(t)$, is due to the inertia associated with mass (m) or weight (W) at time (t) since the onset of ground shaking can be evaluated as follows:

$$F_h(t) = a_h(t) \times W \qquad (2)$$

Where, $$a_h(t) = \frac{A_h(t))}{g} \qquad (3)$$

$A_h(t)$ = Magnitdue of the horizontal ground acceleration at time (t) acting on the soil mass being analzyed for stablity acting in the direction opposite to the direction of the force $F_h(t)$.

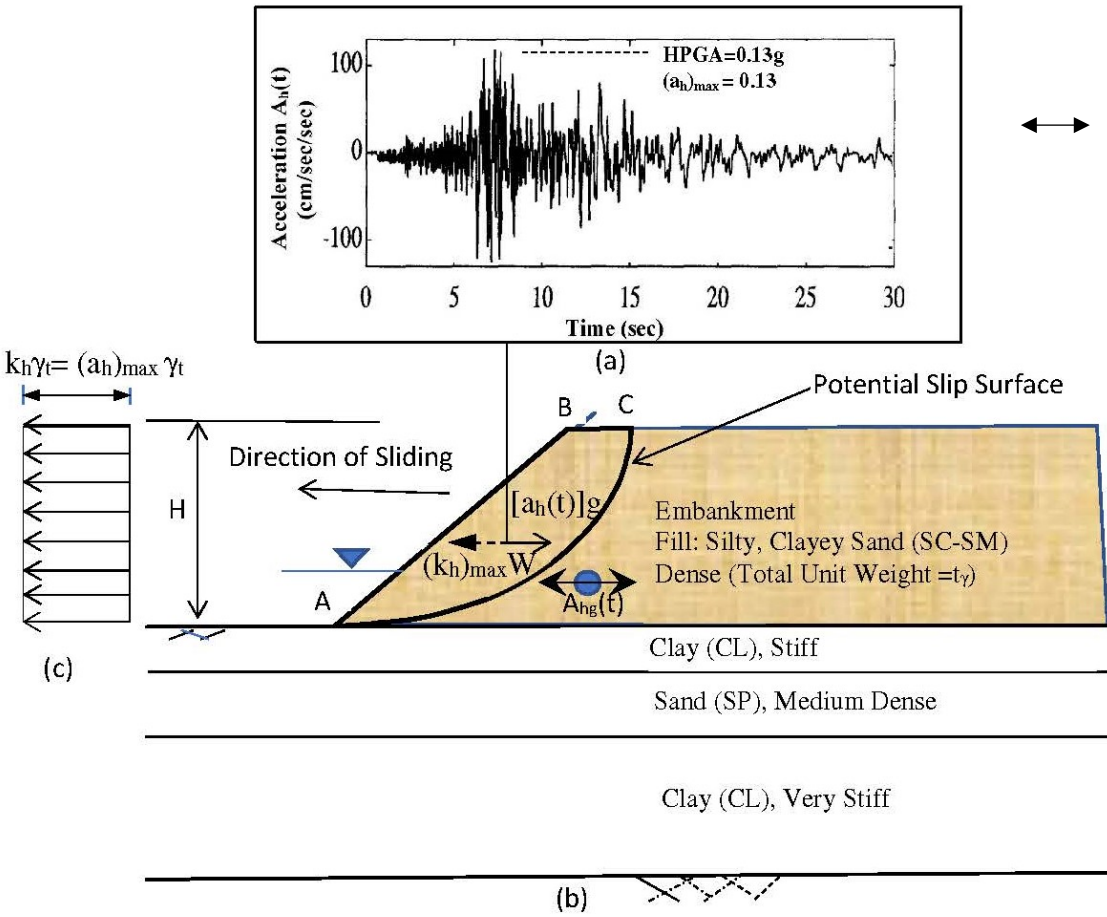

Schematic Model for Pseudo-Static Slope Stability Analysis of a Slope; (b) Example of a Horizontal Acceleration-Time History Measured at the Ground Surface (Horizontal Peak Ground Acceleration (HPGA)=0.13g; and (c) Sustained Horizontal Ground Acceleration. $(k_h)g = (a_h)_{max}\,g$ for Pseudo-Static Lateral Stability Evaluation.

W = Total weight of the potential sliding mass

g = Acceleration due to gravity, and

t = Time starting from the onset of ground-shaking

The parameters $a_h(t)$ is the coefficient of horizontal acceleration $A_h(t)$ at time (t). Note that units for the various parameters defined above must be consistent with the unit used for the acceleration due to gravity, g.

Based on Equation 3, the maximum value of the coefficient $a_h(t)$ for a horizontal acceleration-time history with a peak acccleration of $(A_h)_{peak}$ is given by:

$$(a_h)_{max} = \frac{(A_h)_{peak}}{g}$$

As an example, for the ground motion shown in Figure 3(a), which acts at the centriod of the mass of the soil for which sliding stability along the slip surface shown is being analyzed:

$$(a_h)_{max} = \frac{(A_h)_{peak}}{g} = \frac{128\ cm/sec/sec}{980\ cm/sec/sec} = 0.13$$

In a limit-equilibrium based pseudo-static slope stability type analysis, the commulative effects of the dynamic lateral forces, $F_h(t)$, acting on the soil mass during the entire ground shaking period are presented by applying sustained (i.e., similar to a static force) constant magnitude lateral force on the soil mass acting in the direction of potential lateral instability. This force is termed as the "pseudo-static" force to distinguish its dyamic nature from that of the static loads. The magnitude of this single equivalent pseudo-static interial lateral force, (F_h) is calculated as follows, where conventionally the parameter k_h is used in place of the parameter to $(a_h)_{max}$ to represent the commulative affects of the acceleration-time history [$A_h(t)$] as discussed above.

$$F_h = k_h W \qquad (4)$$

The parameter k_h is the coefficient of the equivalent pseudo-static horizontal ground acceleration, or simply the "Seismic Coefficient".

The value of the parameter k_h or $(a_h)_{max}$ corresponding to the maximum value of pseudo-static force $(F_h)_{max}$ that the soil mass can support without sliding is termed as the coefficient of the yield acceleration, designated herein as $(k_h)_y$. For given and specific strength conditions (e.g., drained, undrained, liquefied, non-liquefied etc), the parameter $(k_h)_y$ represents its capacity against lateral sliding in terms of the coefficient of the peak ground acceleration, $(A_h)_{peak}$, that a soil mass can support without sliding. That is, the parameters $(k_h)_y$ can be thought of as the "capacity coeffcient" in terms of seismic coefficient" for a slope or ERS. In the literature this coefficient of the yield acceleration is often shown as k_{yield}, k_y, or k_c etc.

In a GLE based pseudo-static slope and overall (or global) stability of ERS, unless specified otherwise for unusually high slopes or ERS, the earthquake-induced ground motion represented by $A_h(t)$ is assumed to act uniformly througout the soil mass for which stability is being analysed. Similarly, the equivalent horizonal pseudo-static ground acceleration, represented by k_h, is also assumed to act uniformly through the soil mass contained within the slip surface, as shown schematically in Figure 3.

The horizontal acceleration-time history [$A_h(t)$] assumed to be acting uniformly on the soil mass being analyzed can be considered as the average ground motion that has been transfered from the basement soil through a shear zone of finite thickness (the slip surface).

The earthquake-induced average ground motion at the top of basement soil on which sliding, if any, will occur is thus the input motion. The input or the basement ground motion can be represented by acceleration-time history $A_{hg}(t)$. The corresponding values

of the coefficient of the input horizontal ground accelerations at the top of the basement soil as a function of time can be determined as follows:

$$a_{hg}(t) = \frac{A_{hg}(t)}{g}$$

The maximum value of the coefficient $a_{hg}(t)$ for an input acceleration-time history with a peak acccleration of $(A_{hg})_{peak}$ is given by:

$$(a_{hg})_{max} = \frac{HPGA\ at\ the\ top\ of\ the\ basement\ soil}{g} = \frac{(A_{hg})_{peak}}{g}$$

For a pseudo-static lateral stability analysis, the parameter $(a_{hg})_{max}$ can be thought of as the "demand coefficient" in terms of the coefficient of the input (basement) peak ground acceleration, $(A_{hg})_{peak}$.

In general, for a soil mass or ERS to be considered stable against lateral sliding, it is necessary that:

Capacity Coefficient ≥ Demand Coefficient

or, $$(k_h)_y \geq (a_{hg})_{max} \quad (5a)$$

Alternatively, the soil mass or ERS will be considered susceptible to lateral instability, if

$$(k_h)_y < (a_{hg})_{max} \quad (5b)$$

For SEE, the design ground motion represented by the parameters "Design HPGA" and "Design M" is the input (or basement) ground motion. That is,

$$(a_{hg})_{max} = \frac{Design\ HPGA\ (in\ g)}{g}$$

The coefficient $(a_{hg})_{max}$ corresponding to the Design HPGA is represented in the literature using various symbols, including k_{max} or a_{max}.

Thus, for SEE design:

1) A soil mass or ERS will be considered stable against lateral sliding, if

$$(k_h)_y \geq \left(\frac{Design\ HPGA}{g}\right) \quad (6a)$$

2) Alternatively, the soil mass or the ERS will be considered susceptible to lateral instability, if

$$(k_h)_y < \left(\frac{Design\ HPGA}{g}\right) \quad (6b)$$

However, as discussed earlier, unless a soil mass is affected by flow type liquefaction and to such extent that the total available minimum lateral resistance corresponding to the undrained residual shear strength (S_r) of the liquefied soil layer(s) falls below the total destablizing static lateral force, the relative sliding displacement during any loading cycle will stop soon after the input (basement) ground motion falls below the yield acceleration $(k_h)_y g$. The soil mass will regain a stable condition relative to the basement soil mass although shaking is continued, until after the next cycle when instataneous input acceleration [A_{hg}(t)] exceeds $(k_h)_y g$ again. The soil mass will experience additional relative displacement during this cycle but like earlier, the relative displacement will stop soon after the value of instataneous input acceleration [A_{hg}(t)] drops below $(k_h)_y g$.

The relative sliding displacement occurring during a given loading cycle for which [A_{hg}(t)] excceded $(k_h)_y g$ will be a relatively small amount. These relative lateral displacements occuring during each such cycle will accumulate. However, after each of these cycles the soil mass will regain its lateral stablity. The soil mass will achieve and maintain a relative stable condition after the last lateral displacement producing loading, which is likely to occur well before the cessation of ground shaking.

As will be discussed later, the amount of total relative sliding displacement that a soil mass may experience due to the input ground motion event depends on the ratio of the yield acceleration $(k_h)_y g$, and the peak ground acceleration [A_{hg}(t)] ($(k_h)_y / a_{hg}$), and the duration of ground shaking, which is a measure of the earthquake magnitue (M_w).

Based on the criteria expressed by the Equation 6 above, for SEE design, a slope or an ERS (including bridge abutments) will experience lateral instability or lateral sliding displacements if $\frac{(k_h)_y}{(\frac{Design\ HPGA}{g})} < 1.0$. However, for SEE design this does not necessarily mean that the slope or the ERS does not meet seismic design requirement to prevent failure or collapse. First it only means the ground or the earth structure will experience lateral displacements during the design seismic event. The soil slope, ERS or bridge abutment may displace laterally by a certain minimum amount (Δ_{min}) before it will be considered being failed or collapsed that would pose a threat to life-safety. This minimum displacement (Δ_{min}) is equivalent to the displacement capacity $\Delta_{capacity}$ specified in a displacement-based seismic design. In this case, the seismic design criterion can be expressed as:

$$\frac{\Delta}{\Delta_{capacity}} \leq 1.0 \qquad (7)$$

Where, Δ is the calculated lateral displacement due to the design ground motion (HPGA, M). Therefore, given a value for $\Delta_{capacity}$, a lateral displacement analysis will be necessary for a slope or an ERS when a pseudo-static slope stability analysis indicates that:

$$\frac{(k_h)_y}{(\frac{Design\ HPGA}{g})} < 1.0.$$

Pseudo-Static Lateral Slope Stablity Analysis

Pseudo-static slope stability analyses should be based on a Generalized Limit Equilibrium (GLE) based pseudo-static slope stablity analysis method. A computer program is usually used to perform GLE based pseudo-statc slope stability analyses. Similar to a static slope stability analysis, the user needs to select a resonable potential sliding mechanism(s) based on the site-specific topographic and subsurface conditions and other slope/soil mass loading and resistance characteristices, and then a range of kinematically feasible potential slip surfaces for each value of coefficent k_h.

Results of a GLE based pseudo-static analysis are expressed in terms of a factor of safety (FS) against sliding. It is the ratio of the available stabilizing total lateral nominal resistance to the total destabilizing lateral load acting in the direction of potential sliding. The final result of a set of pseudo-static slope stablity analyses (runs) performed for a given k_h value, all other conditions remaining the same, is a minimum factor of safety (FS_{min}) and a corresponding most critical slip surface.

To evaluate the lateral stability directly due to the design ground motion, this analysis is performed with k_h = (Design HPGA)/g.

If the results of this analysis indicate a $FS_{min} \geq 1.0$, the slope or the soil mass analyzed is considered stable against lateral instability during the design ground motion event. For an unsupported slope, a $FS_{min} \geq 1.0$ also indicates that the slope, for the purposed of SEE design, is not susceptible to any lateral deformation or liquefaction-induced lateral spreading. If the results of the above analysis indicate a $FS_{min} < 1.0$, the slope or soil mass analyzed is considered susceptible to lateral ground deformations or spreading displacements, but not necessarily to collapse or failure for the purpose of SEE design. In this case, additional analyses are necessary involving stablity and lateral deformations, as discussed below.

Example: Pseudo-Static Slope Stablity Analysis

Results of an example GLE based pseudo-static slope stablity analysis performed for a variation of the slope shown in Figure 3 are in Figure 4.

The selected soil parameters for this example soil profile are in Table 1.

Table 1. Soil Parameters

Layer No.	Soil Description	Unit Weight	Soil Strength Parameters		
			Short-Term	Long-Term	Seismic
1	Fill: Silty Sand (SM), with clay, dense	125	c= 500 psf ϕ= 34^o	c'=200 psf ϕ= 34^o	c=500 psf ϕ= 34^o
2	Clay (CL), stiff	128	S_u=1500 psf	c'=300 psf ϕ= 30^o	S_u=1500 psf
3	Sand (SP), medium dense	110	c= 100 psf ϕ= 35^o	c= 0.0psf ϕ= 35^o	Liquefied S_r =700 psf
4	Clay (CL), very stiff to hard	130	S_u= 2700 psf	c'=500 psf ϕ= 28^o	S_u= 2700 psf

The design ground motion parameters for this example are: Design HPGA = 0.6g and Design M_w = 7.5

It is assumed that that there is no groundwater and no liquefaction hazard. The short-term soil parameters presented in Table 1 are applicable. This example analysis uses the GLE based Morgenstern-Price method. A FS_{min}= 0.81 was obtained (Figure 4).

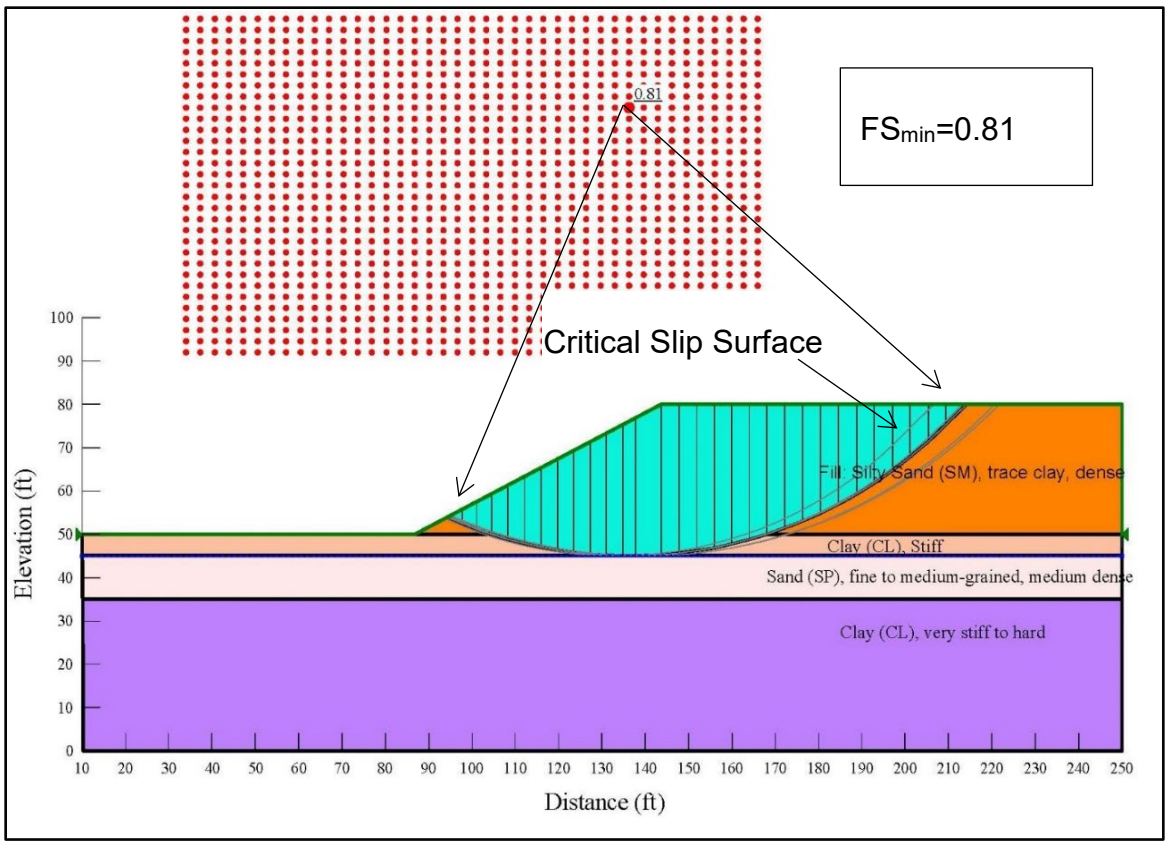

Figure 4. Results of An Example Pesudo-Static Slope Stablity Analysis

The above value of the FS_{min} indicates that the example slope is susceptible to lateral sliding during the design ground motion event. Unlike static design, this does not not necessarily constitute a failure or collapse for SEE seismic design. Further analyses and evaluations (discussed below) are necessary to estimate the amount of sliding displacement that the soil may experience during the design ground motion event.

Pseudo-Static Horizontal Yield Acceleration

For a given soil mass, a set of pseudo-static slope stability analyses can be performed by varying the value of the seismic coeffcient k_h, while all other factors remain the same. This will result in a set of FS_{min} values, one for each of the selected values of k_h. Results of such an analysis for the slope in Figure 4 are in Table 2.

Table 2. Results of Pseudo-Static Analyses for Yield Acceleration

k_h	FS_{min}
0.0	2.56
0.1	2.02
0.2	1.61
0.3	1.30
0.4	1.07
0.5	0.92
0.6	0.81

The above results can be plotted to determine the value of k_h corresponding to FS_{min}=1.0 (Figure 5). The value of k_h =0.44 corresponding to FS_{min}=1.0 is the coefficient of the pseudo-static horizontal yield acceleration $(k_h)_y$ defined earlier. For the above slope, (kh)y=0.44.

The slip surface associated with the yield acceleration $[(k_h)_y]g$ =0.44g, as shown in Figure 6, is the *most critical slip surface for this slope since this is the surface* along which sliding will occur during all seismic shaking events during which the input peak ground acceleration $[(a_{hg})_{max}]$ exceeds the yield acceleration $[(k_h)_y]g$, including the above SEE "Design Earthquake" event.

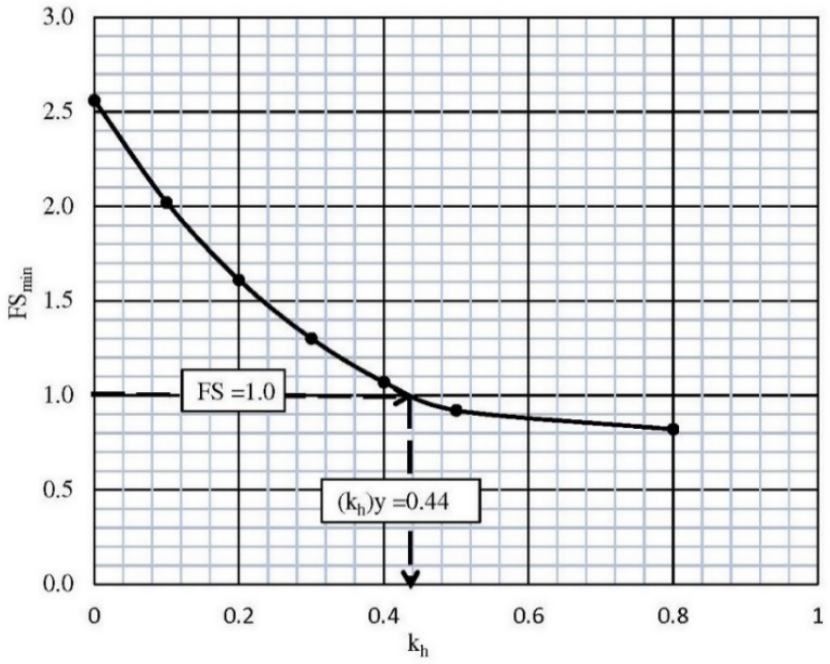

Figure 5. Determination of the Cofficient of Yield Acceleration

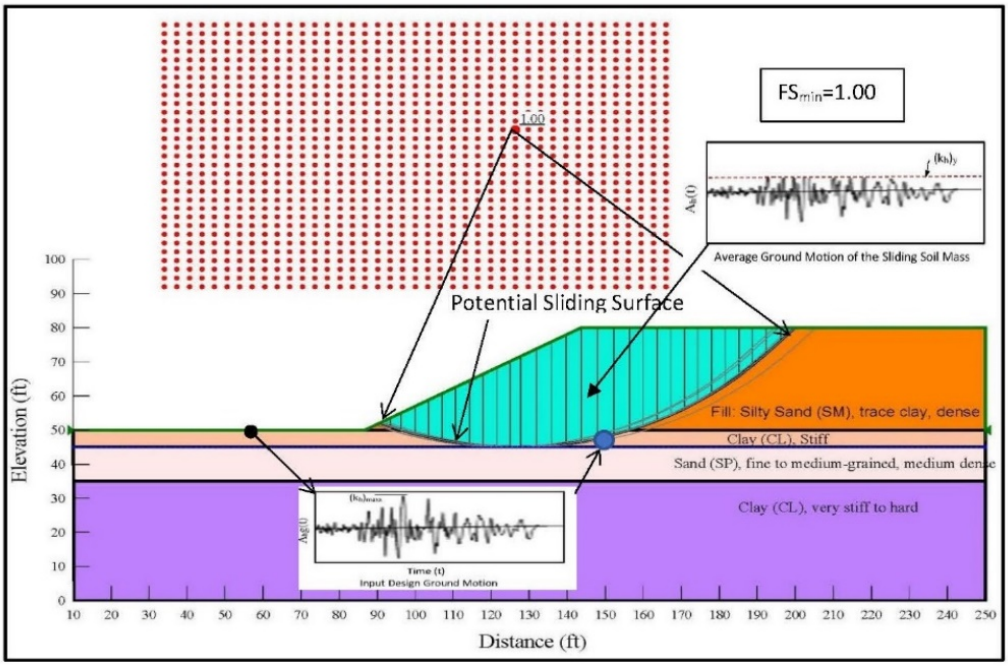

Figure 6. Determination of the Coefficient of the Yield Acceleration and Sliding Surface

As expected based on FS_{min} = 0.81 (Figure 4), the coefficient of yield acceleration or the capacity coefficient $(k_h)_y$ = 0.44 is less than the demand or the maximum coeffcient of the input peak ground acceleration, $(A_{hg})_{max} = (\frac{Design\ HPGA}{g}) = 0.6$

For the given slope and the magnitude of the available total nominal lateral resistance, the coefficent $(k_h)_y$ and the associated sliding surface are unique in the sense that neither depends on the input or the design ground motions.

Note that as seismic pseduo-static slope stability analyses are currently performed, the slip surfaces, even for a given slope and lateral resisting conditions, vary with the magnitude of the input horizontal peak ground acceleration (k_h). Based on the above discussion on the uniqueness of the sliding surface, for a given slope and lateral resistance condition, it is recommend that when performing pseudo-static slope stability analyses for all values k_h, the slip surface be fixed to “sliding surface” associated with the yield acceleration. For given slope, any change in the lateral resisting strength parameters will result in a change of the value of $(k_h)_y$ as well as the corresponding “sliding surface”.

Based on the above analysis, for this design:

$$(k_h)_y \leq (\frac{Design\ HPGA}{g})$$

Thus, further analysis is necessary to estimate lateral displacements that may occur by sliding during the design seismic ground motion event.

Newmark Displacement Analysis Method (NDAM)

Newmark (1965) proposed a very simple method for estimating the co-seismic relative lateral displacement between a finite, rigid mass of soil resting on the surface of a semi-infinite, rigid basement soil mass, when the later is subjected to an earthquake-induced ground motion event.

Due to the simplifications involved with this analysis method, the displacement estimated based by NDAM was intended to be used as an index, rather than as a specific value, for assessing the degree of the potential hazards associated with the co-seismic relative lateral movements between the soil mass and the basement soil. Furthermore, the direction of the relative lateral displacement estimated using NDAM is assumed to be horizontal, irrespective of the directions of the slip surface.

Newmark deformation is purely plastic deformation occurring by sliding. No elastic deformation that may occur prior to the onset of plastic deformation is considered in this analysis. For soil-to-soil sliding sliding only surface, any eleastic deformation should be small and may be neglected.

However, for a soil mass restrained by external supported mechnical elements, in particular by deep foundations, the amount of lateral deflection or deformation that may occur prior to reaching the plastic state of deformation assumed in the Newmark method may be significant. That is, a pile supported soil mass (e.g., bridge abutment) does not experience any Newmark type lateral displacement until a plastic hinge is formed in the pile (assuming soil does not flow around the pile). Significant lateral deflection or deformation will occur before the plastic hinge is formed. This lateral deformation is not durectly accounted for directly in the Newmark-type analysis. Furthermore, a plastic hinge forms in a pile when total lateral force (static +seismic) exceeds the pile nominal lateral resistance (R_N). Once the plastic hinge forms, any attempt to increase the total lateral force on the pile will result in a Newmark-type lateral sliding displacement since the soil-mass must have already reached the plastic state in order for the pile to deflect laterally by the amount necessary to form a plastic hinge.

The total lateral force on the pile will never exeeed R_N during any seismic event. R_N is also equal to the maximum lateral resistance that the pile will offer to the soil mass during an earthqauke. It should be noted the k_h value at which the system yielding occurs and Newmark type displacements start of occur is the equal to the coeffcient of the yield acceleration $(k_h)_y$ for the piles-soil mass system. As stated earlier, $(k_h)_y$ represents the lateral capacity of the system, and

A complete seismic lateral displacement analysis using the NDAM comprises of two types of analysis: a force-based analysis (peudos-static slope stability analysis), and a displacement-based analysis.

Step 1: Pseudo Lateral Stability Analysis to Determine Yield Acceleration $(k_h)_y g$

The procedure for evaluating the yield acceleration of a sloped soil mass that may be susceptible to lateral sliding displacements during the design ground motion event is presented earlier.

This section briefly discusses this procedure for a generalized soil-mass KLMN (Figure 7a), which can be used as a convenient tool to discuss the main features of the NDAM.

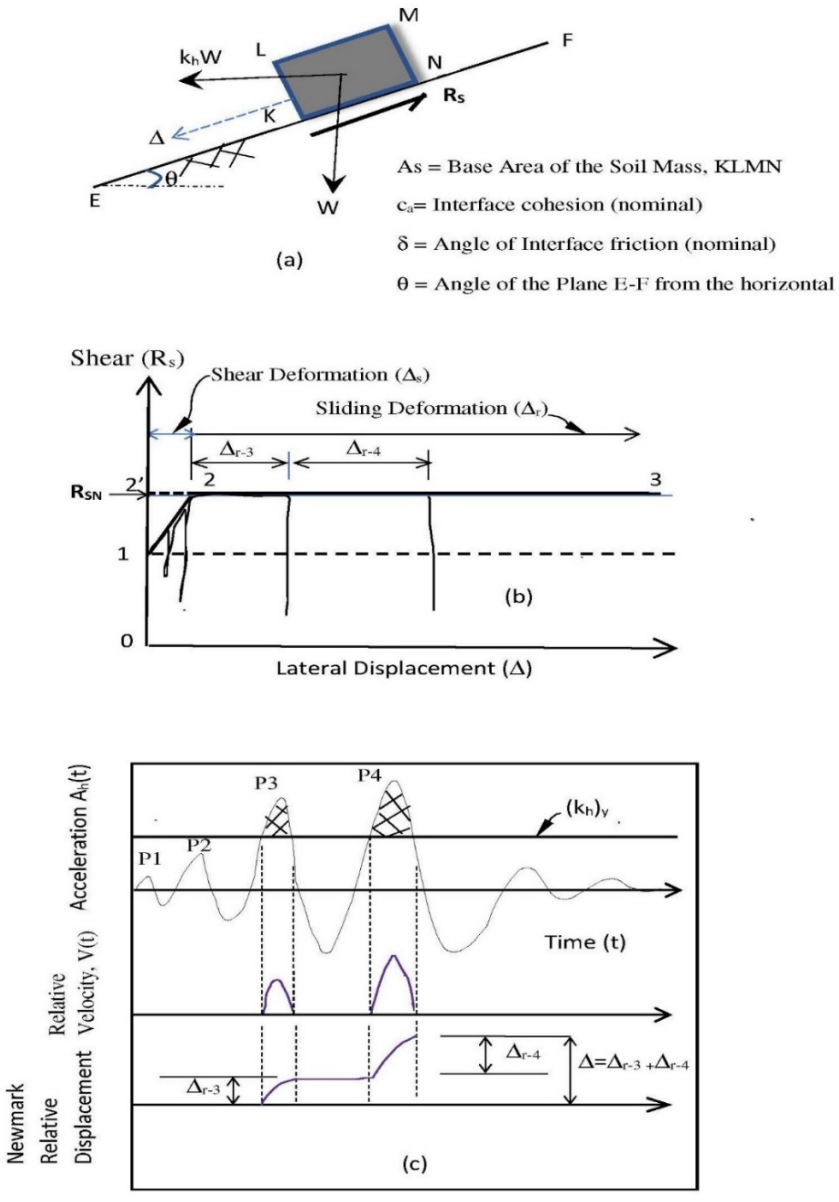

Figure 7. Schematic Diagram Depicting: (a) Newmark's Rigid Soil Mass on an Inclined Plane; (b) Interface Shear -Lateral Displacement Relationship;(c) Newamrk's Rigid Body Type Cosesimic Displacement (Δ).

In Figure 7(a), the potential lateral effects on the soil mas KLMN of ground shaking during an earthquake-induced ground motion event, similar to the pseudo-static stability analysis discussed above, is respresented by a pseudo-static lateral force ($k_h W$) acting horizontally to the left. It is assumed that the soil mass is stable against sliding in the upslope direction.

The pseudo-static factor of safety against lateral sliding stability of the soil mass KLMN along the interface NM in Figure 7(a) is:

$$FS = \frac{R_{SN}}{R_{Total}} \qquad (8)$$

Where, R_{SN}= total nominal lateral resistance of the soil mass, and R_{total}= total destabilizing lateral load acting on the soil mass

By solving Equation (8) for FS_{min} = 1.0, the coeffcient of the pseudo-static yield acceleration $(k_h)_y$ for the soil mass KLMN can be evaluated. If $(k_h)_y$> (Design HPGA/g) lateral sliding is indicated, the Newmark displacement analysis continued as discussed in the next step.

Step 2: Rigid Body Type Cosesimic Lateral Displacement

The step involves estimation of the co-seismic relative lateral displacement between the soil mass KLMN of weight W and basement soil mass. For this analysis, the input ground motion to the base of the soil mass KLMN is the design ground motion $A_{hg}(t)$ evaluated or specified at the surface (EF) of the basement soil mass at a point just below the base of the soil mass KLMN.

Stability against downslope sliding is provided by the shear resistance (R_s) mobilized on the interface or contact surface between the soil mass KLMN and the slope EF.

In general, the mobilized soil-to-soil interface shear resistance (R_s) versus shear deformation (Δ) relationships are non-linear. In practical applications, such a relationship is often simplified in the form of a bi-linear elasto-plastic curve. For lateral stability or large deformation analyses, such as the NDAM, such this relationship is often further simplified to a single horizonal line, which represents a perfectly-plastic interface shear behavior.

For this example, the interface undrained shear resistance-deformation relationships, R_s (Δ), when the soil mass KLMN is subjected to a monotonically applied shear force in the downslope, is shown in Figure 7(b). The simplified bi-linear R_s (Δ) relationship is represented by the lines “1-2” and “2-3” in Figure 7(b), where “1” represents the initial state or static shear component due to gravity ($W\sin\theta$) acting on the soil mass in the direction of potential sliding. Line 1-2 represents lateral displacement due to shear

deformation of the interface shear zone. Displacement beyond Point 2 occurs by sliding along a slip plane.

For soil-to-soil shearing, lateral deformation A'B due to pure shear is usually small (on the order of 0.1" to 0.4"). As noted earlier, this deformation due to pure shear is neglected in the NDAM, and the interface shear (R_s) versus lateral deformation (Δ) relationship is assumed to be represented by the line "2'-2-3" in Figure 7(b). This perfectly-plastic shear resistance-deformation relationship can be expressed as follows:

$$R_S(\Delta) = R_{SN} \quad (9)$$

In practice, the design horizontal ground motion $A_{hg}(t)$ is assumed to be the same as the free-field design ground motion evaluated or specified at the ground surface of a project site. For this discussion, it is assumed that the acceleration-time history shown schematically in Figure 7 (c) represents the design ground motion $A_{hg}(t)$. The positive horizontal direction of the accelerations shown in Figure 7(c) corresponds to the right (opposite to the direction of k_hW), as shown in Figure 7(a).

For these conditions, as soon as the base slope starts to experience ground motion, such as that shown in Figure 7(c), the soil mass KLMN will instantaneously experience the same ground motion resulting in the pseudo-static inertial loads $k_h(t)W = A_{hg}(t)W$. During the initial period the ground shaking is usually low in magnitude. For an interface characterized by a bi-linear shear-deformation relationship, such as the one represented by the points 1-2-3 in Figure 7(b), the soil mass KLMN is likely to experience some small lateral displacements due to shear deformation of the soils within an interface shear zone of finite thickness.

However, the maximum lateral movement of the soil mass KLMN due to the above shear deformation will remain $\leq \Delta_c$ as long as $R_{Total} \leq R_{SN}$. This condition is depicted in Figure 7(b) during the time the basement slope during the 1st and 2nd cycles of positive acceleration respresented by peak accelerations P-1 and P-2 in Figure 7(c). Shear deformation will also occur during the initial portion of the 3rd positive acceleration cycle until the time when R_{Total} becomes equal to R_{SN}, corresponding to $A_{hg}(t) = (k_h)y$.

A discussed earlier, for a given slope if the value of R_{SN} does not change during ground shaking, the value of the parameter $(k_h)_y$ will remain the same during the ground motion event. In that case, the corresponding yield acceleration $[(k_h)_y]g$ versus time (t) can be respresented by a straight line as shown in Figure 7(c). This line represents the maximum value of the coefficient k_h (t) or A_{hg} (t) that the soil mass KLMN can be subjected to without any sliding at the interface.

At any instant during shaking of the basement slope, $A_{hg}(t)$ becomes equal to $(k_h)_y$, which results in $R_{Total} = R_{SN}$, the interface is stressed to the yield condition as shown in Figure 7(b). At this point, any attempt to increase R_{Total} to a value greater than R_{SN} will cause downslope sliding movement along the interface.

In Figure 7(c), the above condition occurs for the first time during the 3rd cycle of positive acceleration starting at time $t_{1\text{-}1}$ and persisting until $t_{1\text{-}2}$ during which $A_{hg}(t)g$ remains greater than $[(k_h)_y]g$. Based on NDAM, due to shear yielding condition of the interface, during this time period the input acceleration $A_h(t)$ acting on the soil mass KLMN remains limited to $(k_h)_y$. This results in differences in the accelerations of soil mass KLMN and the basement slope causing differences in their velocities, which in turn results in relative movements between the two bodies by sliding along the interface slip plane

The relative velocity-time history, as shown on the middle panel of Figure 7(c), due to the 3rd cycle of basement slope acceleration, is obtained by integrating the hatched base acceleration-time history starting from $t_{1\text{-}1}$ and ending at $t_{1\text{-}3}$ at which point the relative velocity drops to zero. The corresponding Newmark Displacement ($\Delta_{r\text{-}3}$) is obtained by integrating the relative velocity from time $t_{1\text{-}1}$ to $t_{1\text{-}3}$. Once the relative velocity drops to zero, the two soil masses move together and no additional Newmark Displacement occurs until the positive basement slope acceleration $A_{hg}(t)g$ exceeds $[(k_h)_y]g$ again. For this example in Figure 7, this happens again during the next or the 4th cycle of positive acceleration cycle. The calculations performed for the 3rd cycle are then repeated to evaluate Newmark Displacment ($\Delta_{r\text{-}4}$) occurring due to the the 4th cycle of positive accelerations with peak P-4.

The cumulative Newmark Displacement at end of the 4th cycle of positive acceleration can be obtained by adding $\Delta_{r\text{-}3}$ and $\Delta_{r\text{-}4}$. The Newmark Displacements, if any, occurring during the subsequent cycles of positive basement accelerations are calculated in a similar manner, and the total Newmark Displacement (Δ) at the end of ground shaking is calculated by summing the Newmark Displacements ($\Delta_{r\text{-}i}$) estimated for each of the cycles during which $A_{hg}(t)g$ exceeds $[(k_h)_y]g$. For this example, in Figure 7, the positive basement acceleration does not exceed $[(k_h)_y]g$ during the remainder of the ground shaking period, and thus no additional sliding deformation occurs. The total Newmark Displacement (Δ) is thus obtained by summing $\Delta_{r\text{-}3}$ and $\Delta_{r\text{-}4}$ as shwon in Figure 7(c).

The maximum or the peak ground acceleration that a sliding soil mass is subjected is limited to the yield acceleration $[(k_h)_y]g$ as shown Figure 7.

Evaluation of Newmark Displacement Using Empirical Correlations

Newmark Displacement (Δ) can be estimated by using published empirical correlations. At this time, the use of the following empirical correlation (Bray and Tavasarou (2007)) is recommended:

$$\Delta\,(\text{inches}) = 0.3937\,\text{Exp}[-0.22 - 2.83\,\text{Ln}(k_h)_y - 0.333\,\{\text{Ln}((k_h)_y)\}^2 + 0.566\,Ln((k_h)_y)\,Ln((a_{hg})_{max}) + 3.04\,Ln((a_{hg})_{max}) - 0.244\,\{\text{Ln}((a_{hg})_{max})\}^2 + 0.278(M-7)] \quad (10)$$

For clarity, in the above correlation the original symbols k_y and PGA used in Bray and Tavasarou (2007) are replaced with the symbols $(k_h)_y$ and $(a_{hg})_{max}$, respectively. For the Department's projects, when the design ground motion is specified or evaluated at the ground surface in accordance with the procedure in the SDC, no modification to any of the design ground motion parameters, including $(a_{hg})_{max}$ (which is equal to the design PHGA/g), is necessary for use in the above correlation or any other such empirical correlations.

Equation 10 provides the estimated median lateral displacement (Δ). The estimated lateral displacement range is 0.5Δ to 2.0Δ.

Due to the sigificant simplified assumptions and the uncertanities involved with the above analysis procedures, it is recommended that any lateral displacement estimate less than 1.0 inch should be considered as equal to zero (i.e., no lateral spreading or displacement).

Liquefaction-Induced Flow Failure

Steeply sloping ground, and ERS or retained earth are under the influence of sustained (or static), destabilizing gravity-induced lateral forces compared with their available stabilizing nominal lateral resistances. Such grounds are particularly susceptible to lateral instability during seismic ground motion events. For example, landslides along steeply sloping mountains sides are common occurrences during strong motion events.

Past observations after large earthquakes indicted that steep slopes and retained-earth adjacent to near water bodies such as those associated with ports, dams, levees, and the banks of rivers and other water bodies are particularly prone to very large lateral ground displacements which, once initiated, occur under the action of gravity alone like flow type aseismic landslides.

Flow failure of a soil masses during earthquakes can occur when the available total lateral resistance drops, due to liquefaction, below the total static driving force.

At this time, a GLE based pseudo-static slope stability type analysis, as discussed earlier, is usually performed to evaluate if a soil mass is susceptible to liquefaction-induced flow failure. For this analysis, the available total lateral resistance of the soil mass or the ERS is evaluated based on the undrained residual strength of the soils that are predicted to liquefy when subjected to the design ground motion. The potential effects of soil liquefaction in the available lateral nominal resistance of lateral resisting elements, if any, such as deep foundations and ground anchors, also need to be considered.

The pseudo-static slope stability analysis for this purpose is performed by the setting, k_h=0.0 and using undrained residual shear strengths for the liquefied soil layer(s)

The soil mass analyzed is considered susceptible to liquefaction-induced flow failure if the results of this analysis indicate a FS_{min}<1.0. Otherwise, the soil mass is considered not susceptible to flow failures.

In the lateral case, the soil mass may still be susceptible to liquefaction-induced lateral spreading and needs to be further analyzed as discussed earlier.

Lateral displacements due to flow failures are usually very large. A practical method to estimate lateral flow displacement is not available currently. For design, it is assumed that a soil mass susceptible to flow failure is likely to experience large movements which for all practical purposes will constitute a failure or collapse, and thus need to be avoided. This can be achieved by improving or modifying the conditions of the potentially liquefiable soil to reduce or eliminate liquefaction hazards, and/or by using deep foundations to increase the available total lateral nominal resistance.

Liquefaction-Induced Lateral Spreading Displacements

Researchers have used several approaches, including empirical or semi-empirical correlations, numerical analysis and physical modeling, to estimate lateral ground deformations or displacements due to earthquakes. Most of these approaches are applicable to non-liquefied free-field ground conditions. Due to the complexities involved, both the tools available for and their capabilities to estimate liquefaction-induced lateral spread displacements during future earthquakes are very limited.

Unless specified otherwise in a project specific seismic design criteria, the following simplified methods may be used to estimate liquefaction-induced lateral spread displacement for most regular projects.

Liquefaction-Induced Lateral Spread Displacements for Free-Field Conditions

The following analysis procedures may be used to estimate liquefaction-induced free-field lateral displacement involving the third category of lateral spreading discussed in the liquefaction induced lateral spreading section.

Hamada et al (1986) Procedure

Hamada et al (1986) proposed the following simple empirical relationship, which may be used for rough or initial estimates of the free-field liquefaction-induced lateral displacements for the ground shown in Figure 9.

$$\Delta = 0.75\, H^{1/2}\theta^{1/3} \qquad (12)$$

Where, Δ = Permanent ground displacement in the lateral (horizontal) direction (m)

H= Thickness of the liquefied soil layer (m)

θ = The larger gradient of the ground surface or the lower boundary face of the liquefied soil layer (%)

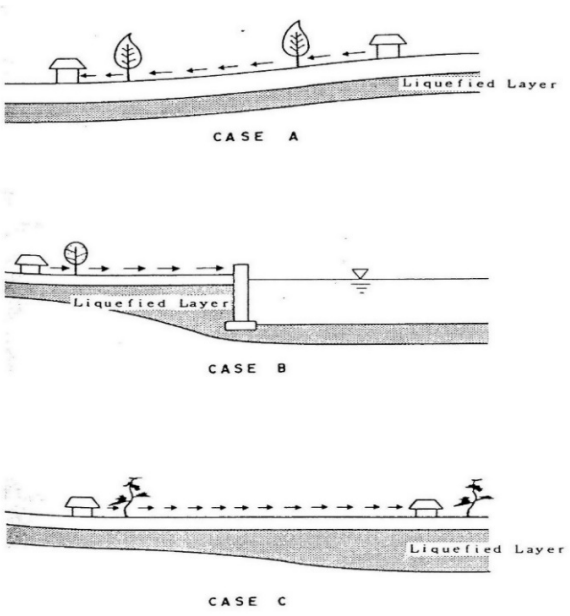

Figure 9. Types of Permanent Ground Displacements (Hamada et al., 1986)

When using Equation (12), the lateral ground displacements in the field should be expected to range from about ½ Δ to 2Δ . Based on Hamada et al (1986), in some of the field case histories used in the development of the Equation (12), lateral ground moments continued to occur after the cessation of the ground shaking.

Multilinear Regression (MLR) Procedure

Bartlett and Youd (1992, 1995) and Youd et al (2002) developed more details for the prediction of free-field liquefaction-induced lateral spread displacements. In the development of these empirical correlations, lateral spread in the simplest form is defined as the riding of a non-liquefied surficial soil layer or crust on a directly underlain liquefied soil layer either gently sloping ground toward a free face (i.e., not supported by any mechanical means, such as ERS) unsupported) downward grade change, such as that occurred due to incised river, canal, creek, lake, ponds, bluffs or other sudden depressions within an otherwise relatively flat area. The basic mechanisms involved with the above definition of lateral spread are depicted in Figure 9, although the associated mechanisms in the field are far more complex.

Bartlett and Youd (1995) found that liquefaction-induced lateral spread displacement is a function of earthquake, topographical and soil factors. Youd et al (2002) developed two different empirical correlations to estimate liquefaction-induced free-field lateral spread displacement (Δ), one for gently sloping ground (with no free face) condition and the other for both sloped and flat ground with a free face condition as presented in the following sections.

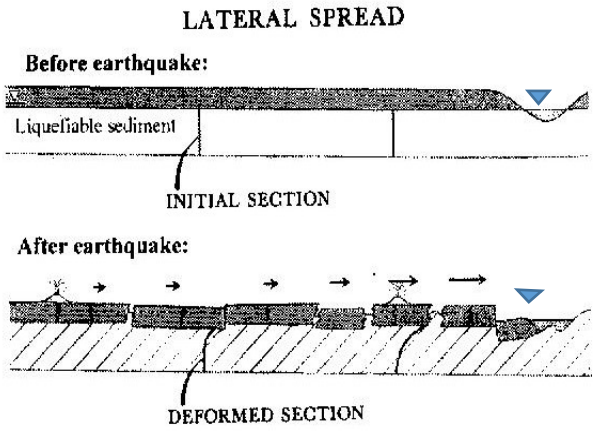

Figure 10. Liquefaction-Induced Lateral Spread (Youd, 2018)

Gently Sloping Ground Condition

The liquefaction-induced free-field lateral (horizontal) spread ground displacement (Δ in meters) in this case, which involves soil mass movements down a gently sloping ground, may be estimated based on the following empirical correlation:

$$Log\,\Delta = -16.213 + 1.532M - 1.406\,log\,R^{*} - 0.012\,R + 0.338\,log\,S + 0.540\,log\,T_{15} + 3.413\,log\,(100 - FC_{T15}) - 0.795\,log\,(D50_{T15} + 0.1\text{ mm}) \quad (13)$$

The various parameters in Equation (13) are defined in the following section. For these conditions, in addition to soil liquefaction-induced reduction in the shear strength of the underlying liquefiable soil layer(s), sustained or static lateral destabilizing mass forces due to gravity acting on lateral spread soil mass in the direction of the slope play a significant role.

Free-Face Ground Conditions

The following empirical correlation is recommended to estimate the lateral (horizontal) ground displacement (Δ in meters) toward a free face, as defined above:

$$Log\,\Delta = -16.713 + 1.532M - 1.406\,log\,R^{*} - 0.012\,R + 0.592\,log\,W + 0.540\,log\,T_{15} + 3.413\,log\,(100 - FC_{T15}) - 0.795\,log\,(D50_{T15} + 0.1\text{ mm}) \quad (14)$$

Where, $R^{*} = R_0 + R$ and $R_0 = 10^{(0.089\,M_w - 5.64)}$, and

$R=R_{rup}$ = mean site-to-fault rupture surface distance (km); T_{15} = cumulative thickness (m) of liquefied soil layers with corrected blow counts $N1_{60}$ <15; FC_{T15} = average fines (passing US #200 sieve) content (%), of the liquefied soil layers included in the T_{15} calculations; $D50_{T15}$ = average mean grain size (mm), of the liquefied soil layers included in the included T_{15} calculations; S = ground slope (%), and W = free-face ratio (%), defined as the ratio of the height (H) of the free-face to the horizontal distance (L) from the toe of the free face to the point on the ground Δ is evaluated for, as shown in Figure 11.

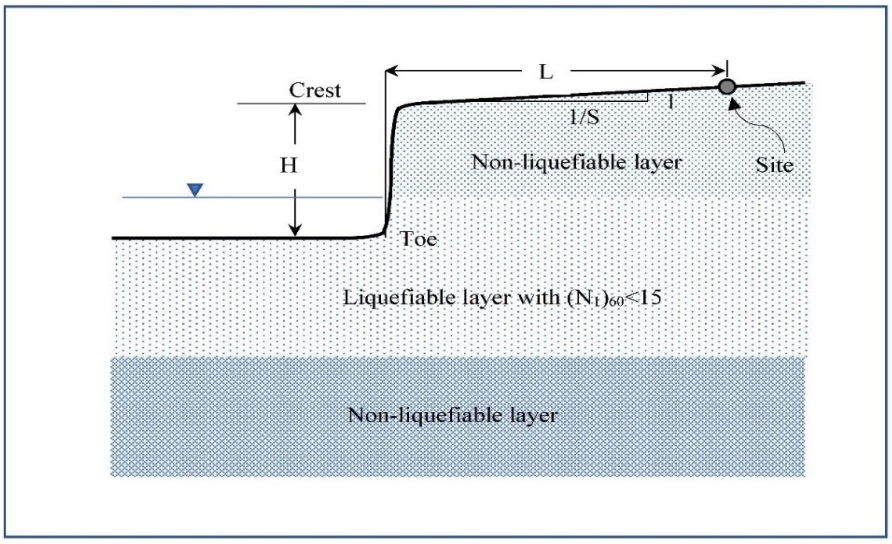

Figure 11. Model Parameters (Modified after Bartlett and Youd, 1992)

Seismic Lateral Displacement Analysis for Slopes and Earth Retaining Structures

The NDAM is used to perform lateral spreading hazards for mildly (> 6 %) to steeply sloping slopes, ERS and bridge abutments.

Externally Unrestrained Slopes and ERS

The NDAM method is used to estimate liquefaction-induced lateral displacements of moderate (> 6 %) to steeply sloping ground and ERS not restrained or stabilized by means of externally founded structural elements such as piles, tiebacks and ground anchors. These ERS include gravity walls and conventional, semi-gravity type reinforced concrete walls founded on shallow foundations, and internally stabilized walls, such as soil nail and mechanically stabilized earth walls and geosynthetic-reinforced walls.

For these ERS, two types of lateral stability and displacement mechanism need to be considered: (1) Overall or global stability using GLE based pseudo-static slope stability method as discussed earlier, and (2) Lateral sliding along the base using pseudo-static limit-equilibrium analysis of the forces and resistances in the lateral or horizontal direction. In this analysis, the seismic inertial force acting on the ERS or ERS-backfill composite sliding mass is calculated using the seismic coefficient (k_h), and the yield acceleration capacity $(k_h)_y$ is calculated based on a FS=1.0 against lateral sliding, in a similar manner discussed above for slopes.

The lower of the two $(k_h)y$ values, one based on the overall or global stability and second based on the lateral sliding stability along the base, will control the lateral sliding failure of the wall, and thus is yield capacity of the ERS in term of seismic coefficient. This lower value of $(k_h)_y$ is used to calculate lateral displacement using NDAM in the similar manner discussed above for a slope, for which there were only one $(k_h)_y$ value.

Externally Restrained Slopes and ERS

Liquefaction-induced lateral ground displacement analysis for externally restained ground and ERS is of major significance for several transportation systems. These systems include bridge supports founded on piles and ERS supported vertically on and/or laterally supported by deep foundations and anchored walls.

In concept, NDAM for these systems is very similar to the laterally unrestrained systems or slopes as presented above. The main difference is that lateral stability and lateral spreading displacement analyses need to incorporate the lateral nominal resistance offered by the external restraining elements on lateral stability and lateral spreading displacements. The total lateral nominal resistance is the sum of the lateral nominal resistances of the soil and the externally restained elements.

Once the lateral nominal resistance per unit width of the slope or ERS is determined, it can be applied as an additional lateral resisting force on the potential sliding soil-mass. One major complexity is that the two lateral nominal resistances are not moblized at the same lateral displacement. As discussed the soil mass is considered rigid and the sliding material is characterized as perfectly plastic. This means that no lateral displacement occurs prior to the mobization of the soil lateral nominal resistance or yield condition. This assumption is considered reasonable for soils but not for external restraining elements such piles. Significant lateral deformation of the pile is necessary before its lateral nominal resistance is mobilized.

The piles in these cases derive their lateral resisting capacities on the soils below the potential sliding surface, which in turn depends on the magnitude of the lateral resistance offered by the piles. The restraining element and the soil mass interact in a complex manner.

Additional difficulties arises due to nature and timing of ground motion and soil liquefaction, and interaction with other elements, for example the superstucture and the abutment wall in the case of a bridge abutment founded on piles.

In summary, lateral spread hazard analyses for these sytems are very difficult due to the complex nature of the interactions between soil and the external restaints, and the phenomena of earthquake motions and soil liquefaction, and other factors.

Due to the above complexities, the state of knowledge and practical analysis procedures are limited and evolving rapidly. At this time, simplifying assumptions must be made to be able to develop practical lateral spreading displacement analyses for these types of structures. However, to be acceptably reliable, even the simplest of the methods require some modeling and numerical soil-structure-interaction analyses.

The Department's currently recommended procedure for estimating liquefaction-induced lateral spreading displacements at bridge supports with deep foundations is in MTD 20-15 (2017). An example lateral spreading analysis using the procedure in MTD 20-15 is included herein.

Until ERS specific analysis procedures are available, the procedure may be used to perform liquefcation-induced lateral spreading hazard for other types of externally restained ERS.

Other Analysis Methods for Estimating Lateral Spread Displacements

Researchers have been using physical modelling and numerical methods to study the phenomenon of liquefaction-induce lateral spreading. While the results of such studies are useful to understand the basic mechanisms and identify the factors, due to the complexities involved, their applicability as well as reliability at this time are limited for use in the design of routine projects. Use of numerical methods requires special expertise, skills and tools, and may be considered for large and complex projects in consultation with the structure designer.

Hazard Mitigation Strategies

As discussed earlier, deep foundations are considered the most appropriate for supporting bridges at sites susceptible to liquefaction-induced lateral spreading hazards during earthquakes. One of the main reasons for this is that a pile foundation not only to transfers loads to deeper, usually more competent soils, it also provides additional lateral nominal resistances to the potentially laterally unstable soil mass. In some cases, use of pile foundations needed to support other loads may be adequate to limit or even prevent any lateral spreading displacements. In all cases, provided the deep foundation is embedded into the foundation soils below the moist critical slip surface by length not less than the critical length (L_c), as defined in the MTD 3-1, will provide some mitigation. The

critical length (L_c) in this case must be evaluated by ignoring lateral resistances from the soils above the most critical slip surface.

Ground improvements, with or without deep foundations, may be used to reduce or even eliminate lateral spreading hazards. Ground improvements may be targeted to reduced or eliminate liquefaction hazards and/or provide additional lateral resistance to the soil mass susceptible to lateral spreading. Ground improvement methods may include: removal and replacement of liquefiable soils with compacted fills, dynamic compaction, stone columns, soil mixing and grouting.

References

1. Crandall, Roderic, 1908, The San Francisco Peninsula, in The California Earthquake of 1906: Carnegie Inst. Washington, v.1, p. 246-254.
2. Hobbs, W. H. (1908), A Study of the Damage to Bridges During Earthquakes, The Journal of Geology, Vol. 16, No. 7, pp. 636-653.
3. Dutton, C. E. (1890), The Charleston Earthquake, 9th Annual Report, U.S. Geological Survey, Washington DC.
4. Grogan, W. P., and Vallerga, B.A. (2000), Earthquake Damage and Repair of Oakland Airport Runway, Journal of Performance of Constructed Facilities, Vol. 14, No. 4, November, ASCE, Washington DC
5. Nakata, J.K. et al (1999), The October 17, 1989, Loma Prieta, California, Earthquake—Selected Photographs, Photographs and descriptions to accompany, Digital Data Series DDS-29, Version 1.2. Accessed at https://pubs.usgs.gov/dds/dds-29/dds-29.pdf
6. Oldham, R. D. (1899), Report of the Great Earthquake of 12th June 1897, Memorial Geological Survey of India, Vol. XXIX.
7. Robertson, P. K., (2009), Evaluation of Flow Liquefaction and Liquefied Strength Using the Cone Penetration Test, Journal of Geotechnical Engineering, ASCE, Vol. 136, No. 6, June.
8. Seed, H. B., Idriss, I. M, (1971), Simplified Procedure for Evaluating Soil Liquefaction Potential, Journal of the Soil Mechanics and Foundation Division, ASCE, Vol. 97, No. SM9, September.
9. Seed, H. B., Idriss, I. M, and Arango, I (1983), Evaluation of Soil Liquefaction Potential Using Field Performance Data, Journal of Geotechnical Engineering, ASCE, Vol. 109, No. 3, March.
10. Youd, T. L., 1971, Landsliding in the vicinity of the Van Norman Lakes in The San Fernando, California, earthquake of February 9, 1~71: U.S. Geol. Survey Prof. Paper 733, p. 105-109.
11. Youd, T. L. (1973), Liquefaction, Flow, and Associated Ground Failure, Geological Survey Circular 688, USGS, Washington DC.
12. Youd, T. L. (1993), Liquefaction-Induced Damage to Bridges, Transportation Research Record 1411, Washington D.C.
13. USGS (1992), The Loma Prieta, California, Earthquake of October 17, 1989, Marina District, Strong Ground Motion and Ground Failure, USGS Processional Paper 1551-F, Edited by Thomas O'Rourke, Washington.
14. Wei. X. et al (2008), Damage Patterns and Failure Mechanisms of Bridge-Pile-Foundation Under Earthquake, The 14th World Conference on Earthquake Engineering October 12-17, 2008, Beijing, China.
15. Wood, H. O., 1908, Distribution of apparent intensity in San Francisco, in The California Earthquake of April 18, 1906: Carnegie Inst. Washington, v. 1, p. 220-246.